

Applicability of multi-component study on Bayesian searches for targeted anisotropic stochastic gravitational-wave background

Soichiro Kuwahara¹ and Leo Tsukada^{2,3,4,5}

¹*Research Center for the Early Universe (RESCEU),
The University of Tokyo, Tokyo 113-0033, Japan*

²*Department of Physics, The Pennsylvania State University, University Park, PA 16802, USA*

³*Institute for Gravitation and the Cosmos, The Pennsylvania State University, University Park, PA 16802, USA*

⁴*Department of Physics and Astronomy, University of Nevada,*

Las Vegas, 4505 South Maryland Parkway, Las Vegas, NV 89154, USA

⁵*Nevada Center for Astrophysics, University of Nevada, Las Vegas, NV 89154, USA*

Stochastic background gravitational waves have not yet been detected by ground-based laser interferometric detectors, but recent improvements in detector sensitivity have raised considerable expectations for their eventual detection. Previous studies have introduced methods for exploring anisotropic background gravitational waves using Bayesian statistics. These studies represent a groundbreaking approach by offering physically motivated anisotropy mapping that is distinct from the Singular Value Decomposition regularization of the Fisher Information Matrix. However, they are limited by the use of a single model, which can introduce potential bias when dealing with complex data that may consist of a mixture of multiple models. Here, we demonstrate the bias introduced by a single-component model approach in the parametric interpretation of anisotropic stochastic gravitational-wave backgrounds, and we confirm that using multiple-component models can mitigate this bias.

I. INTRODUCTION

The stochastic gravitational-wave background (SGWB) is a super-position of numerous gravitational waves whose sources are not individually resolved. Several astrophysical and cosmological processes have been proposed as contributing to the gravitational-wave background (GWB). The astrophysical sources include, for instance, large numbers of distant binary black holes (BBHs), binary neutron stars (BNSs) [1–6], magnetars [7–9], and core-collapse supernovae [10–14]. On the other hand, cosmological sources include cosmic strings [15–18], gravitational-waves (GWs) emitted during the inflationary era [19–21], and primordial black holes (PBHs) [22–24].

Recently, the Advanced LIGO Observatory (aLIGO) [25] and Advanced Virgo [26] detectors have completed the third observing run (O3) and the first period of the fourth observing run (O4a), collaborating with KAGRA [27]. The ground-based GW detectors have not made any detection of the GWB [28]. However, in the nanohertz frequency band, where ground-based GW detectors are not sensitive due to seismic noise, pulsar timing array (PTA) collaborations have reported a potential signal in the form of a GWB-induced quadrupolar correlation of timing residuals [29].

The promising results from PTA collaborations emphasize the importance of searching for not only isotropic but also anisotropic GWB. Some models of the aforementioned astrophysical or cosmological sources imply characteristic angular distributions [30–40]. Additionally, persistent point sources such as Scorpius X-1 [41, 42] might also be observable through the detection techniques developed for anisotropic GWB. The LIGO, Virgo, and KAGRA (LVK) collaboration reported the

results of their search for anisotropic GWB [43]. They introduced three analysis techniques: broadband radiometer analysis (BBR) [44, 45], narrow band radiometer analysis (NBR) [46], and spherical harmonic decomposition (SHD) [47], derived from cross-correlation techniques and the choice of orthonormal basis.

Inspired by SHD analysis, Tsukada *et al.* [48] presented a Bayesian parameter estimation approach for a targeted anisotropic GWB. While the conventional SHD analysis approach, which was applied in the LVK collaboration search [43], estimates each spherical-harmonic mode using regularization techniques, Tsukada *et al.* [48] formalized the analysis assuming a specific anisotropy model to be known and estimated its parameters. Although their approach is groundbreaking in terms of physically motivated mapping techniques of anisotropy, the search is limited by employing a single model. As reported in [48, Appendix A], since we do not know the anisotropy model present in the real sky *a priori*, choosing the wrong spatial scale of a background or an incorrect model can potentially lead to bias in the parameter estimation. There are several spectral separation searches on isotropic or anisotropic GWB [49–51]. Also, spectral separation analysis on the data from the first three LVK observing runs is performed by [52]. Those studies focus on the difference in the known spectral indices of the signals. In this search, we would like to introduce the separation search on multi-targeted \mathcal{P}_{lm} distribution to keep the benefit of being not bothered by Fisher matrix regularization. We assume the realistic situation that isotropic background exists on top of the target anisotropy and display the bias induced by choosing a single component recovery model. We finally demonstrate that applying multi-component recovery model would mitigate the bias by examining the probability-probability plot generated from its poste-

rior distribution to prove the necessity of introducing the multi-component analysis on this Bayesian approach. As a by-product, in Sec.IV, we also present the Bayes-factor heat maps and a histogram to quantitatively address the preference of models with the different cases of signal appearance or different noise realization.

II. FORMALISM

A. Likelihood

The basic Bayesian formalism idea for an anisotropic SGWB is stated in Ref.[48]. Additionally, Tsukada [53] expanded the likelihood formalism for the mixture model of different polarization. This formalism can be used for a mixture of anisotropy models. We can write the mixture of models of a detector response, meaning the expectation value of the cross spectral density (CSD), as

$$\langle C(f, t) \rangle = \sum_i \sum_\mu \gamma_\mu(f, t) \mathcal{P}_\mu^i(f, \vec{\theta}) \quad (1)$$

where i represents each signal components and μ represents (l, m) basis since we choose spherical-harmonics basis to decompose the skymap in this search. The definition of CSD is the cross-correlated data from two detectors at the frequency f and the time coordinate t , and its formulation is given below:

$$C(f, t) \equiv \frac{2}{\tau} \tilde{d}_1(f, t) \tilde{d}_2^*(f, t) \quad (2)$$

where the $\tilde{d}(f, t)$ is the Fourier transformation of detector output $s(t)$ computed in an interval $[t - \tau/2, t + \tau/2]$.

γ_μ is an overlap function of the detector network for μ basis [54] and its multiplication shows up as detector response of the signal. In the weak signal approximation and assuming no cross-correlated noise between detectors, the covariance matrix of CSD can be approximated as a diagonal matrix [55] given by

$$\begin{aligned} \Sigma_{CC'} &\equiv \langle |C(f, t)|^2 \rangle - |\langle C(f, t) \rangle|^2 \\ &\approx \delta_{tt'} \delta_{ff'} P_1(f, t) P_2(f, t) \end{aligned} \quad (3)$$

where $P_k(f, t)$ is the power spectral density (PSD) of the k -th detector centered around t .

According to the factorization given in Ref. [48, 53], assuming the target anisotropy model can be decomposed into frequency spectrum factor $H(f, \vec{\theta})$ and sky-map factor in spherical-harmonic basis \mathcal{P}_{lm} , it follows that

$$\mathcal{P}_{lm}(f, \vec{\theta}) = \epsilon \bar{H}(f, \vec{\theta}) \bar{\mathcal{P}}_{lm}. \quad (4)$$

$\bar{H}(f, \vec{\theta})$ and $\bar{\mathcal{P}}_{lm}$ are normalized as

$$\bar{H}(f, \vec{\theta}) \equiv \frac{H(f, \vec{\theta})}{H(f_{\text{ref}}, \vec{\theta})}, \quad (5)$$

$$\bar{\mathcal{P}}_{lm} \equiv \frac{\mathcal{P}_{lm}}{\mathcal{P}_{00}}. \quad (6)$$

Also, ϵ is normalized by $\frac{3H_0^2}{2\pi^2 f_{\text{ref}}^3 \sqrt{4\pi}}$ so that the amplitude parameter ϵ is compatible to $\hat{\Omega}_{\text{GW}}$ of LVK's isotropic search [28, 56, 57]. Given multiple signal component \mathcal{M} , the form of Gaussian likelihood becomes almost identical to Eq.21 in Ref.[53] except we consider tensor mode only in this paper

$$p(C_{ft} | \epsilon_i, \vec{\theta}_i; \mathcal{M}) = \frac{1}{(2\pi)^{N_{\text{dim}}/2} \sqrt{|\Sigma_{CC'}|}} \exp \left\{ -\frac{1}{2} \sum_{f,t} \frac{\tau \Delta f |C(f, t) - \sum_i \epsilon_i \bar{H}_i(f, \vec{\theta}_i) \gamma_\mu(f, t) \bar{\mathcal{P}}_\mu^i|^2}{P_1(f, t) P_2(f, t)} \right\}. \quad (7)$$

For implementing this Bayesian analysis, we used and further developed the pipeline used in Ref. [48, 53] which utilizes the `Bilby` package [58, 59]. Since the integration over multi-dimensional parameter space is required for the computation of posterior distribution and evidence as shown in Eq. 7, we adopt a nested sampling algorithm package called `Dynesty` [60].

The computation of Eq.(7) requires two-dimensional integration over frequencies and time segments, and it requires significant computational time. Ref.[48] introduces the implementation of precomputing and storing the time integration part beforehand. Additionally, Ref.[53] formulates the extra components of pre-computable part in the presence of multiple signal com-

ponents from various polarization modes. Here, we basically follow the same computation as in Ref.[53] but only consider the tensor mode with multiple anisotropic signal components. Taking the logarithm of Eq.(7), the exponent part appears as

$$\begin{aligned} &-\frac{1}{2} \sum_{f,t} \frac{\tau \Delta f |C(f, t)|^2}{P_1(f, t) P_2(f, t)} + \sum_i \epsilon_i \Re[(\bar{\mathcal{P}}_\mu^i)^* X_\mu^i] \\ &\quad - \frac{1}{2} \sum_i \sum_j \epsilon_i \epsilon_j (\bar{\mathcal{P}}_\mu^i)^* \Gamma_{\mu\nu}^{ij} \bar{\mathcal{P}}_\nu^j \end{aligned} \quad (8)$$

where the indices (μ, ν) corresponds to the summation over spherical-harmonics basis. The definitions of matrix

X_μ^i and $\Gamma_{\mu\nu}^{ij}$ are as follows

$$X_\mu^i = \sum_f \bar{H}_i(f, \vec{\theta}) \sum_t \frac{\tau \Delta f C(f, t) \gamma_\mu^*(f, t)}{P_1(f, t) P_2(f, t)} \quad (9)$$

$$\Gamma_{\mu\nu}^{ij} = \sum_f \bar{H}_i(f, \vec{\theta}) \bar{H}_j(f, \vec{\theta}') \sum_t \frac{\tau \Delta f \gamma_\mu^*(f, t) \gamma_\nu(f, t)}{P_1(f, t) P_2(f, t)} \quad (10)$$

where τ is the duration of the segment where the short Fourier transformation is performed to the time series and Δf is the frequency resolution. The \sum_t part in both equation is precomputed and stored to decrease the amount of computation time.

III. PARAMETER ESTIMATION FOR MULTI-COMPONENT INJECTION

A. Setup

1. \mathcal{P}_{lm} distribution

In order to check the credibility of introducing multi-component recovery model against multi-component injections, we compare the parameter estimation results by applying different recovery models. The injected signals are pure isotropic distribution and mock Galactic-plane distribution. We should note that the Galactic-plane distribution has its monopole component aside with the injected isotropic signal. The recovery models are a single-component recovery model (Galactic-plane) and a two-component recovery model (Isotropic and Galactic-plane). In injecting and recovering the Galactic-plane distribution, we choose consistent $l_{\max} = 5$ as highest l mode. The spherical-harmonics components \mathcal{P}_{lm} for the Galactic-plane is given from the mock distribution used in Fig. 1 of Ref. [48].

2. $H(f, \vec{\theta})$ model

We assume $H(f, \vec{\theta})$ as a power-law model for both injections. The model's parameter set consists of the slope of the spectrum, α ; $\vec{\theta} = \{\alpha\}$.

$$H(f, \alpha) = \left(\frac{f}{f_{\text{ref}}} \right)^{\alpha-3}, \quad (11)$$

where f_{ref} is an arbitrary reference frequency and chosen to be 25 Hz in this study. The index parameter α corresponds to the spectral index of Ω_{GWB} .

3. prior distribution

The free parameters for both injections (Galactic-plane and Isotropic model) are amplitude parameter ϵ and

spectral index α given in Sec. III A 2. We perform 500 analyses on different noise realizations. The injected parameters are generated randomly from prior distribution of the corresponding parameters in the recovery model so that we can obtain a reasonable probability-probability plot on successful parameter estimation. We introduce a log-uniform distribution ranging from 10^{-10} to 10^{-5} for ϵ . For the index α , we introduce a Gaussian distribution with a mean 2 and a standard deviation of 1 since this distribution can cover the cases of $\alpha = 0, 2/3, 3, 4$. $\alpha = 0$ and $\alpha = 3$ are associated with the cosmological SGWB. For example, $\alpha = 0$ corresponds to the SGWB from inflationary era [19–21] or cosmic strings [15–18], and $\alpha = 3$ is associated with the SGWB from core-collapse supernovae [10–14]. The remaining value of $\alpha = 2/3, 4$ are associated with the astrophysical SGWB originating from compact binary coalescence (CBC)s [1–6] and magnetars [7–9] respectively. Those injections are made on the simulated noise CSD of two LIGO detectors for one year of observation. The noise spectrum used for simulated noise is the designed sensitivity for the Advanced LIGO detectors [61].

B. Results

1. Posterior distribution

Fig. 1 is an example of the posterior distribution for two-component recovery when the injection is loud enough to have a large Bayes factor for decisive signal evidence. The injected parameter values are $(\epsilon_0, \alpha_0) \sim (2.88 \times 10^{-6}, 2.9865)$ for Galactic-plane injection indicated by a red star and $(\epsilon_1, \alpha_1) \sim (1.62 \times 10^{-6}, 2.5511)$ for Isotropic injection indicated by an orange star. The vertical dashed line on 1-dimensional histograms shows (0.05, 0.95) percentiles for each distribution and the inner circle of the two-dimensional plot shows 68% contour level while the outer circle is associated with 95% contour level. As is inferred by Fig. 1, the injected values are precisely recovered within an error of $O(0.1)\%$ for the very loud signal. In contrast, Fig. 2, which is an example of posterior distribution for single component recovery against the two-component injection, shows a bias in the recovery. The injected parameter values are $(\epsilon_0, \alpha_0) \sim (8.18 \times 10^{-8}, 2.0/3.0)$ for Galactic-plane injection and $(\epsilon_1, \alpha_1) \sim (4.092 \times 10^{-9}, 0.0)$ for Isotropic injection. The isotropic component of the Galactic-plane signal is recovered with optimal (SNR) ≈ 100 . As the definition of optimal signal-to-noise ratio (SNR), we refer to the Eq.9 of Ref.[62]. Although we inject a very loud Galactic-plane signal and the log of Bayes factor (BF) ($\sim 6.5 \times 10^3$) for recovery shows a significantly high value, its posterior distribution does not recover the target signal.

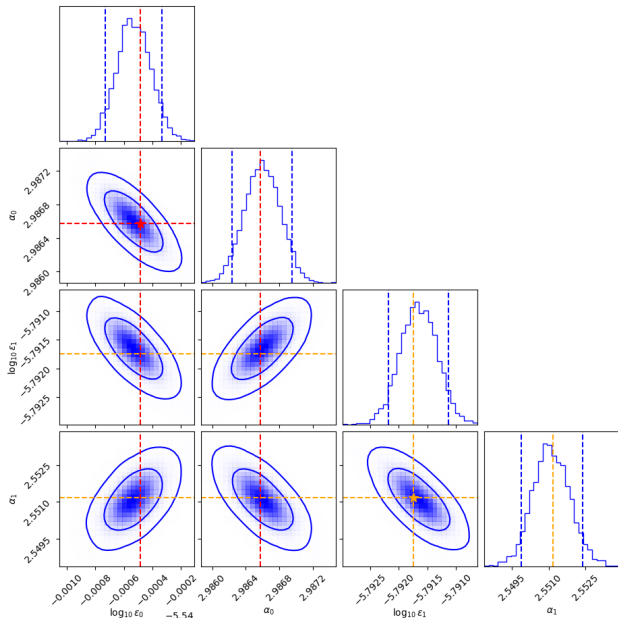


FIG. 1. An example posterior distribution of two-component recovery against two-component injection test with $\ln \text{BF} \sim 1.65 \times 10^8$. The red marker and lines shows the injection parameters for Galactic-plane injection while yellow ones represents those for Isotropic injection.

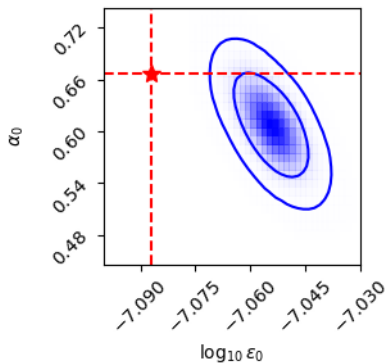


FIG. 2. An example posterior distribution of single-component recovery against two-component injection test. The parameters for Galactic-plane model is recovered only. The red marker and lines shows the injection parameters for Galactic-plane injection. The injection parameter for Isotropic injection is not shown in the figure since it is not the target anisotropy to recover for.

2. Probability-probability plot

We compute the percentile of the injected parameters value along the given posterior distribution in each analysis. We then collect 500 different percentiles from each analysis, sort them in ascending order, and com-

pute the cumulative fraction corresponding to each percentile to create the probability-probability plot. Fig. 3 is the probability-probability plots for two different recovery models against multiple component injection mentioned in Sec.III A 1. For the single component recovery (Galactic-plane), we plot the recovery of injected parameters of the same component which is shown in the left plot of Fig. 3.

IV. MODEL COMPARISON

A. Fixed Noise Realization

Assuming the prior odds for models (let us set \mathcal{M}_1 and \mathcal{M}_2) are equal, the odds ratio is identical to the BF as shown in the following equation

$$\mathcal{O}_{\mathcal{M}_2}^{\mathcal{M}_1} = \frac{p(D|\mathcal{M}_1)p(\mathcal{M}_1)}{p(D|\mathcal{M}_2)p(\mathcal{M}_2)} = \frac{p(D|\mathcal{M}_1)}{p(D|\mathcal{M}_2)} = \mathcal{B}_{\mathcal{M}_2}^{\mathcal{M}_1} \quad (12)$$

where D stands for the data from the detectors. In this section, we describe the significance of a model in comparison with others by the value of BF. According to Ref.[63], evidence against model \mathcal{M}_2 is considered very strong when $\ln \mathcal{B}_{\mathcal{M}_2}^{\mathcal{M}_1} \sim 10$. Also, $\ln \mathcal{B}_{\mathcal{M}_2}^{\mathcal{M}_1} \sim 1$ is described as "not worth more than a bare mention". In order to check the variations in BF along with the difference in injected amplitude of the signals, we let the spectral index parameter α be a fixed value of 0.0 for the Isotropic injections and 0.5 for Galactic-plane injections. In accordance with the injection, a prior distribution of index parameter is set to be a delta function peaking at the injected value. We apply only one noise realization for this analysis using designed sensitivity for Advanced LIGO detectors [61] and injected two-component signals (Isotropic and Galactic-plane) with various sets of amplitude parameter ϵ . Fig.4 are two dimensional heat maps of $\ln \mathcal{B}_N^{\text{SIG}}$ (left) and $\ln \mathcal{B}_{\text{Single}}^{\text{Mix}}$ (right). The left figure is the BF's heat map of multi-component recovery model against noise model. The boundary of $\ln \mathcal{B} \sim 1$ is around $\epsilon \sim 3.2 \times 10^{-9}$ for both components of the injections. The right figure is the BF's heat map of the multi-component recovery model against single component recovery (Galactic-plane) model in the presence of two-component injections. The fluctuation around $\ln \mathcal{B} \sim 1$ comes from the uncertainty of the noise realization because it acts differently in different noise realization. In Fig.5, we inject the same α value of 0.0 across all components while keeping the other parameters—such as amplitude and noise realization—identical to those in Fig.4. This setup allows us to isolate and assess the impact of spectral separation. However, the figure does not clearly reveal a significant effect.

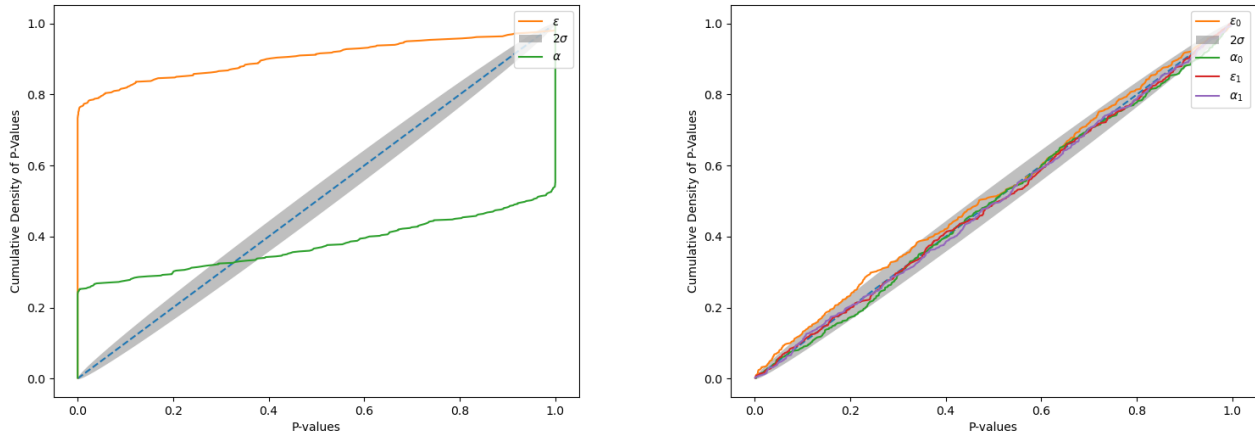


FIG. 3. The probability-probability plot for multiple component injection (Isotropic and Galactic-plane). The left plot corresponds to single component (Galactic plane) recovery and the right plot corresponds to multiple component (Isotropic and Galactic-plane) recovery. In the right plot, index 0 of ϵ and α refers to the parameters of Galactic-plane, and index 1 to that of Isotropic injection. The gray region in both figures is the 2σ credible region expected from applying central limit theorem to binomial distribution.

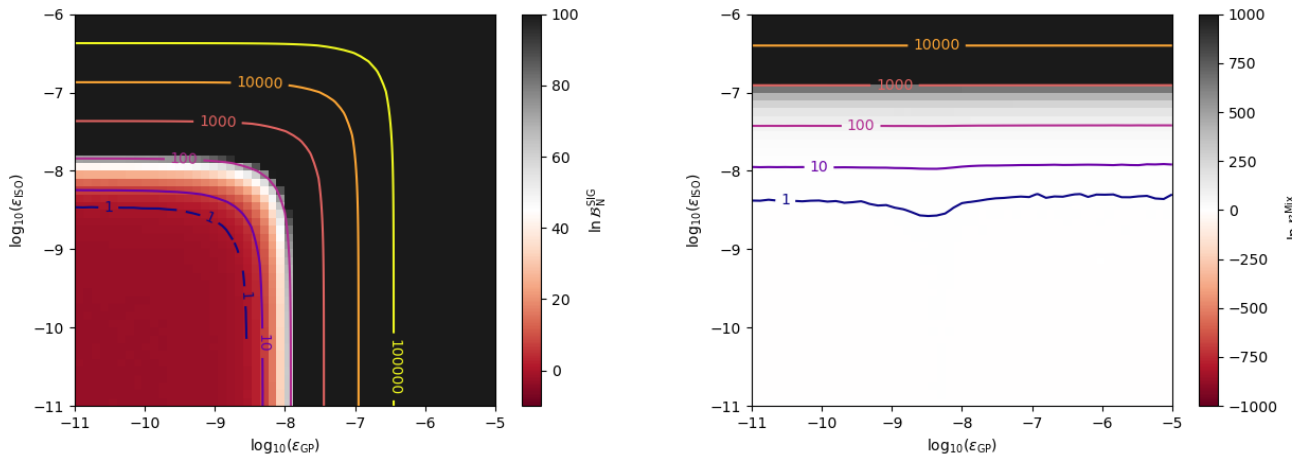


FIG. 4. The two dimensional heat maps for natural logarithm of BF in the case of injecting different sets of amplitude. Left: BF's heat map of multi-component recovery model against noise model. Right: BF's heat map of multi-component recovery model against single component recovery (Galactic-plane) model.

B. Fixed Injections

In this section, we fix the injection amplitude and spectral indices and we change the noise realization by altering seed number. The amplitude parameter is chosen such that the isotropic component of the injected distribution has optimal $\text{SNR} \approx 5$. For the injection of Galactic-plane we inject the parameters $(\epsilon_0, \alpha_0) \sim (4.1 \times 10^{-9}, 2.0/3.0)$, and $(\epsilon_1, \alpha_1) \sim (4.8 \times 10^{-9}, 0.0)$ for the Isotropic injection. We compute the BF for 500 different noise realizations with designed sensitivity of Advanced LIGO detectors [61] used in Sec.III B 2. We also

used the same prior distribution for this analysis, which is a log-uniform distribution ranging from 10^{-10} to 10^{-5} for ϵ and a Gaussian distribution with a mean 2 and a standard deviation of 1 for α . To visualize the distribution of the BF's for each analysis with several recovery models or injection campaign, we plot the histogram of the BF's, which is shown in Fig.6. Comparing with the non-injection case and the two-component injection cases, the BF's for both single- and two-component recovery model against noise model is considerably high. However, the BF's for two-component recovery model have higher value than those for single-component recovery in the presence

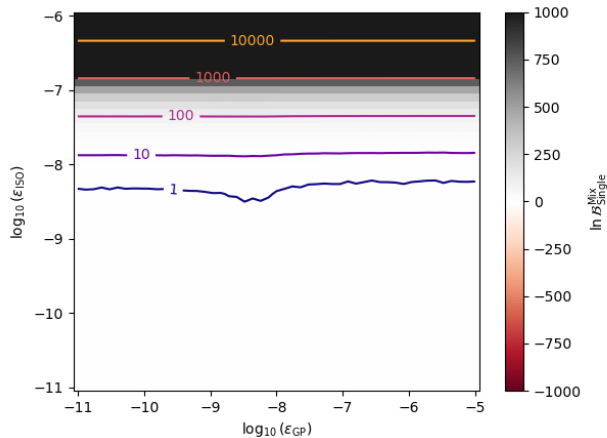


FIG. 5. The two dimensional heat maps for natural logarithm of BF in the case of injecting different sets of amplitude. As a difference we made from Fig.4, we made the injection of α as 0.0 for both injections.

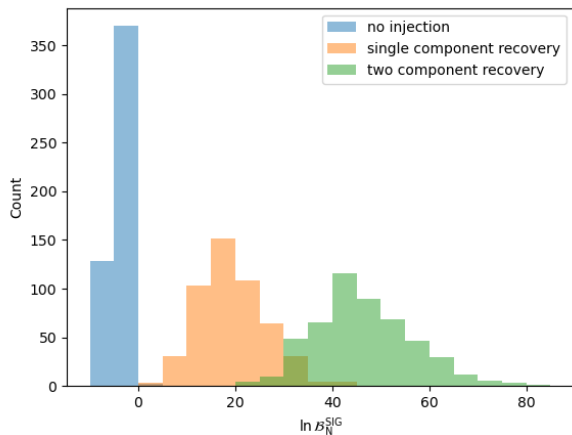


FIG. 6. The histogram of $\ln \mathcal{B}_N^{\text{SIG}}$ for 500 tests with different noise realization each. The blue, orange, and green are corresponding to two-component recovery with no injection, single-component and two-component recovery for two-component injections.

of two-component injections on average which implies

that the former model statistically fits better to the data with injections.

V. CONCLUSION

Sec.IV performs the BF analysis on fixed noise realization and fixed injection. Fig.4 shows that two-component recovery model fits better towards the data. The comparison between Fig.4 and Fig.5 implies that, in our case of anisotropic model, spectral separation does not bring strong impact to the component separation by joint estimation of anisotropy. Fig.6 proves that this feature does not depend on noise realization and can be seen statistically. Even with single-component recovery model, BFs against noise model are very high with a loud signal injection. However, as reported in [48, Appendix. A], choosing the wrong model in recovery may cause the bias in parameter estimation. In this search, we demonstrate multiple component injection (isotropic and anisotropic) and its recovery by choosing different model. We plot the probability-probability plot in Fig. 3. The left plot indicates that single component recovery clearly shows the bias in its parameter estimation as the graph goes outside the 2σ credible region. The right plot shows the validity of posterior results assuming the two-component recovery model. It proves that, in searching for anisotropic GWB with the Bayesian approach presented by [48], choosing a multiple component recovery model (at least including an isotropic model and a targeted anisotropic model) is necessary since it is highly likely that an isotropic GWB exists in the true sky; otherwise, it causes a bias in the parameter estimation.

VI. ACKNOWLEDGEMENT

This work has been supported by Japan Society for the Promotion of Science (JSPS) Grants-in-Aid for JSPS Research Fellow (KAKENHI) grant number JP22KJ1033 and Grant-in-Aid for Scientific Research(A) grant number JP18H03698.

The authors are grateful for computational resources provided by the LIGO Laboratory and supported by National Science Foundation Grants PHY-0757058 and PHY-0823459.

L.T acknowledges support from the Nevada Center for Astrophysics.

[1] T. Regimbau and V. Mandic, *Classical and Quantum Gravity* **25**, 184018 (2008).
 [2] P. A. Rosado, *Phys. Rev. D* **84**, 084004 (2011).
 [3] C. Wu, V. Mandic, and T. Regimbau, *Phys. Rev. D* **85**, 104024 (2012).
 [4] X.-J. Zhu, E. J. Howell, D. G. Blair, and Z.-H. Zhu, *Monthly Notices of the Royal Astronomical Society* **431**,

882 (2013), <https://academic.oup.com/mnras/article-pdf/431/1/882/18243620/stt207.pdf>.
 [5] X.-J. Zhu, E. Howell, T. Regimbau, D. Blair, and Z.-H. Zhu, *The Astrophysical Journal* **739**, 86 (2011).
 [6] S. Marassi, R. Schneider, G. Corvino, V. Ferrari, and S. P. Zwart, *Physical Review D* **84** (2011), 10.1103/physrevd.84.124037.

- [7] T. Regimbau and J. A. de Freitas Pacheco, *Astronomy & Astrophysics* **376**, 381–385 (2001).
- [8] S. Marassi, R. Ciolfi, R. Schneider, L. Stella, and V. Ferrari, *Monthly Notices of the Royal Astronomical Society* **411**, 2549–2557 (2010).
- [9] C.-J. Wu, V. Mandic, and T. Regimbau, *Phys. Rev. D* **87**, 042002 (2013).
- [10] A. Buonanno, G. Sigl, G. G. Raffelt, H.-T. Janka, and E. Müller, *Physical Review D* **72** (2005), 10.1103/physrevd.72.084001.
- [11] E. Howell, D. Coward, R. Burman, D. Blair, and J. Gilmore, *Monthly Notices of the Royal Astronomical Society* **351**, 1237 (2004), <https://academic.oup.com/mnras/article-pdf/351/4/1237/3924132/351-4-1237.pdf>.
- [12] P. Sandick, K. A. Olive, F. Daigne, and E. Van-gioni, *Physical Review D* **73** (2006), 10.1103/physrevd.73.104024.
- [13] S. Marassi, R. Schneider, and V. Ferrari, *Monthly Notices of the Royal Astronomical Society* **398**, 293–302 (2009).
- [14] X.-J. Zhu, E. Howell, and D. Blair, *Monthly Notices of the Royal Astronomical Society: Letters* **409**, L132–L136 (2010).
- [15] S. Sarangi and S.-H. Tye, *Physics Letters B* **536**, 185–192 (2002).
- [16] T. Damour and A. Vilenkin, *Phys. Rev. D* **71**, 063510 (2005).
- [17] X. Siemens, V. Mandic, and J. Creighton, *Physical Review Letters* **98** (2007), 10.1103/physrevlett.98.111101.
- [18] T. W. B. Kibble, *Journal of Physics A: Mathematical and General* **9**, 1387 (1976).
- [19] A. Starobinsky, *JETP Lett.* **30**, 682 (1979).
- [20] M. S. Turner, *Physical Review D* **55**, R435–R439 (1997).
- [21] R. Bar-Kana, *Physical Review D* **50**, 1157–1160 (1994).
- [22] M. Sasaki, T. Suyama, T. Tanaka, and S. Yokoyama, *Phys. Rev. Lett.* **117**, 061101 (2016).
- [23] V. Mandic, S. Bird, and I. Cholis, *Physical Review Letters* **117** (2016), 10.1103/physrevlett.117.201102.
- [24] S. Wang, Y.-F. Wang, Q.-G. Huang, and T. G. Li, *Physical Review Letters* **120** (2018), 10.1103/physrevlett.120.191102.
- [25] J. Aasi *et al.* (LIGO Scientific), *Class. Quant. Grav.* **32**, 074001 (2015), arXiv:1411.4547 [gr-qc].
- [26] F. Acernese *et al.* (VIRGO), *Class. Quant. Grav.* **32**, 024001 (2015), arXiv:1408.3978 [gr-qc].
- [27] T. Akutsu *et al.*, *Progress of Theoretical and Experimental Physics* **2021**, 05A101 (2020), <https://academic.oup.com/ptep/article-pdf/2021/5/05A101/37974994/ptaa125.pdf>.
- [28] R. Abbott *et al.*, *Physical Review D* **104** (2021), 10.1103/physrevd.104.022004.
- [29] H. Xu, S. Chen, Y. Guo, J. Jiang, B. Wang, J. Xu, Z. Xue, R. N. Caballero, J. Yuan, Y. Xu, J. Wang, L. Hao, J. Luo, K. Lee, J. Han, P. Jiang, Z. Shen, M. Wang, N. Wang, R. Xu, X. Wu, R. Manchester, L. Qian, X. Guan, M. Huang, C. Sun, and Y. Zhu, *Research in Astronomy and Astrophysics* **23**, 075024 (2023).
- [30] C. R. Contaldi, *Physics Letters B* **771**, 9–12 (2017).
- [31] A. C. Jenkins, J. D. Romano, and M. Sakellariadou, *Physical Review D* **100** (2019), 10.1103/physrevd.100.083501.
- [32] A. C. Jenkins and M. Sakellariadou, *Phys. Rev. D* **100**, 063508 (2019).
- [33] D. Bertacca, A. Ricciardone, N. Bellomo, A. C. Jenkins, S. Matarrese, A. Raccanelli, T. Regimbau, and M. Sakellariadou, *Physical Review D* **101** (2020), 10.1103/physrevd.101.103513.
- [34] G. Cusin, C. Pitrou, and J.-P. Uzan, *Physical Review D* **96** (2017), 10.1103/physrevd.96.103019.
- [35] G. Cusin, C. Pitrou, and J.-P. Uzan, *Physical Review D* **97** (2018), 10.1103/physrevd.97.123527.
- [36] G. Cusin, I. Dvorkin, C. Pitrou, and J.-P. Uzan, *Physical Review Letters* **120** (2018), 10.1103/physrevlett.120.231101.
- [37] G. Cusin, I. Dvorkin, C. Pitrou, and J.-P. Uzan, *Physical Review D* **100** (2019), 10.1103/physrevd.100.063004.
- [38] C. Pitrou, G. Cusin, and J.-P. Uzan, *Physical Review D* **101** (2020), 10.1103/physrevd.101.081301.
- [39] G. Cañas-Herrera, O. Contigiani, and V. Vardanyan, *Physical Review D* **102** (2020), 10.1103/physrevd.102.043513.
- [40] M. Geller, A. Hook, R. Sundrum, and Y. Tsai, *Physical Review Letters* **121** (2018), 10.1103/physrevlett.121.201303.
- [41] B. P. Abbott *et al.*, *The Astrophysical Journal* **847**, 47 (2017).
- [42] B. P. Abbott *et al.* (LIGO Scientific Collaboration and Virgo Collaboration), *Phys. Rev. D* **95**, 122003 (2017).
- [43] R. Abbott *et al.* (LIGO Scientific Collaboration, Virgo Collaboration, and KAGRA Collaboration), *Phys. Rev. D* **104**, 022005 (2021).
- [44] B. Abbott *et al.* (LIGO Scientific Collaboration), *Phys. Rev. D* **76**, 082003 (2007).
- [45] S. W. Ballmer, *Classical and Quantum Gravity* **23**, S179 (2006).
- [46] S. W. Ballmer, *LIGO interferometer operating at design sensitivity with application to gravitational radiometry*, Ph.D. thesis, Massachusetts Institute of Technology. (2006).
- [47] E. Thrane, S. Ballmer, J. D. Romano, S. Mitra, D. Talukder, S. Bose, and V. Mandic, *Physical Review D* **80** (2009), 10.1103/physrevd.80.122002.
- [48] L. Tsukada, S. Jaraba, D. Agarwal, and E. Floden, *Physical Review D* **107** (2023), 10.1103/physrevd.107.023024.
- [49] A. Parida, S. Mitra, and S. Jhingan, *Journal of Cosmology and Astroparticle Physics* **2016**, 024–024 (2016).
- [50] G. Boileau, A. Lamberts, N. Christensen, N. J. Cornish, and R. Meyer, *Monthly Notices of the Royal Astronomical Society* **508**, 803–826 (2021).
- [51] J. Suresh, D. Agarwal, and S. Mitra, *Physical Review D* **104** (2021), 10.1103/physrevd.104.102003.
- [52] F. D. Lillo and J. Suresh, “Estimating astrophysical population properties using a multi-component stochastic gravitational-wave background search,” (2024), arXiv:2310.05823 [gr-qc].
- [53] L. Tsukada, “Extension of the bayesian searches for anisotropic stochastic gravitational-wave background with non-tensorial polarizations,” (2023), arXiv:2308.09020 [astro-ph.IM].
- [54] B. Allen and A. C. Ottewill, *Physical Review D* **56**, 545–563 (1997).
- [55] J. D. Romano and N. J. Cornish, *Living Reviews in Relativity* **20** (2017), 10.1007/s41114-017-0004-1.
- [56] B. P. Abbott *et al.* (LIGO Scientific Collaboration and Virgo Collaboration), *Phys. Rev. Lett.* **118**, 121101 (2017).
- [57] B. P. Abbott *et al.* (LIGO Scientific and Virgo Collabo-

- ration), *Phys. Rev. D* **100**, 061101 (2019).
- [58] G. Ashton, M. Hübner, P. D. Lasky, C. Talbot, K. Ackley, S. Biscoveanu, Q. Chu, A. Divakarla, P. J. Easter, B. Goncharov, F. H. Vivanco, J. Harms, M. E. Lower, G. D. Meadors, D. Melchor, E. Payne, M. D. Pitkin, J. Powell, N. Sarin, R. J. E. Smith, and E. Thrane, *The Astrophysical Journal Supplement Series* **241**, 27 (2019).
- [59] I. M. Romero-Shaw, C. Talbot, S. Biscoveanu, V. D’Emilio, G. Ashton, C. P. L. Berry, S. Coughlin, S. Galaudage, C. Hoy, M. Hübner, K. S. Phukon, M. Pitkin, M. Rizzo, N. Sarin, R. Smith, S. Stevenson, A. Vajpeyi, M. Arène, K. Athar, S. Banagiri, N. Bose, M. Carney, K. Chatziioannou, J. A. Clark, M. Colleoni, R. Cotesta, B. Edelman, H. Estellés, C. García-Quirós, A. Ghosh, R. Green, C.-J. Haster, S. Husa, D. Keitel, A. X. Kim, F. Hernandez-Vivanco, I. Magaña Hernandez, C. Karathanasis, P. D. Lasky, N. De Lillo, M. E. Lower, D. Macleod, M. Mateu-Lucena, A. Miller, M. Millhouse, S. Morisaki, S. H. Oh, S. Ossokine, E. Payne, J. Powell, G. Pratten, M. Pürrer, A. Ramos-Buades, V. Raymond, E. Thrane, J. Veitch, D. Williams, M. J. Williams, and L. Xiao, *Monthly Notices of the Royal Astronomical Society* **499**, 3295–3319 (2020).
- [60] J. S. Speagle, *Monthly Notices of the Royal Astronomical Society* **493**, 3132–3158 (2020).
- [61] B. P. Abbott and others[†], *Living Reviews in Relativity* **23** (2020), 10.1007/s41114-020-00026-9.
- [62] T. Callister, A. S. Biscoveanu, N. Christensen, M. Isi, A. Matas, O. Minazzoli, T. Regimbau, M. Sakellariadou, J. Tasson, and E. Thrane, *Physical Review X* **7** (2017), 10.1103/physrevx.7.041058.
- [63] R. E. Kass and A. E. Raftery, *Journal of the American Statistical Association* **90**, 773 (1995).